Catalysis Today 303 (2018) 313–319

Contents lists available at ScienceDirect

Catalysis Today

journal homepage: www.elsevier.com/locate/cattod

Effects of shell thickness on Ag-Cu_2O core-shell nanoparticles with bumpy structures for enhancing photocatalytic activity and stability

Changsoo Lee, Kihyun Shin, Yung Jong Lee, Chanwon Jung, Hyuck Mo Lee*

Department of Materials Science and Engineering, KAIST, 291 Daehak-ro, Yuseong-gu, Daejeon, 305-701, Republic of Korea

ARTICLE INFO

Keywords:
Photocatalyst
Surface plasmon resonance
Core-shell nanoparticles
Cuprous oxide
Density functional theory

ABSTRACT

Here we examine Ag-Cu_2O core-shell nanoparticles with bumpy structures for use in plasmonic photocatalysts. We synthesized the nanoparticles using a very simple co-reduction process. The shell thickness of the nanoparticles was controlled in order to investigate the effects of shell thickness on photocatalytic activity and stability. With increasing shell thickness, it was be observed that the activity and the stability were simultaneously improved. A thin shell lead to de-wetting of Cu_2O from the Ag core and considerable oxidation of Cu_2O to CuO. The high activity could be due to the unique structure of Ag-Cu_2O, which has a high surface area and plasmonic charge transfer from the Ag core. In addition, we elucidated the stability tendency using conducted density functional theory (DFT) calculation. Strain induced between the Ag core and shell is critical to the stability, leading to de-wetting and oxidation of Cu_2O.

1. Introduction

Photocatalysts are materials that perform catalytic reactions using light as an energy source [1]. They are utilized for an array of applications, including water splitting [2], CO_2 reduction to hydrocarbons [3], and pollutants removal [4]. The most widely used photocatalyst is TiO_2 (titanium dioxide) because it is earth-abundant, non-toxic, and very stable [5]. However, TiO_2 has very wide band gap of 3.0 eV for the rutile structure [6] and 3.2 eV for the anatase structure [7], which is only active under the ultra-violet region of sun-light. Many researchers have tried to develop alternative materials [8,9] or tried to enhance the photocatalytic activity using strategies such as doping [10,11], light absorbers [12], and mixed oxides [13].

Among many alternative materials, Cu_2O (cuprous oxide), as p-type semiconductor with a direct band gap, has been extensively studied due to its relatively narrower bandgap (2.17 eV) compared to TiO_2 [14]. Similar to the benefits of TiO_2, it is earth-abundant and non-toxic. However, a major portion of the reported Cu_2O nanoparticles show a large size and a relatively small surface area [15]. They also have a weak light absorption at longer wavelength regions of light under 450 nm. Additionally, Cu_2O is naturally oxidized into CuO (cupric oxide) under ambient and aqueous conditions, indicating poor stability of Cu_2O [16].

Using plasmonic light absorber has been proposed as a strategy to enhance the photocatalytic activity of Cu_2O [15]. Nano-sized noble metals such as Au, Ag, and Pt show strong absorption of visible light as a result of their surface plasmon resonance (SPR) property [17]. The absorbed light induces a very strong electric field around the nanoparticles by generating oscillating electrons. The plasmonic light absorber can transfer solar energy into the semiconductor above the conduction band and below the valence band edge, leading to enhanced photocatalytic activity [18]. Ag-Cu_2O core-shell nanoparticles have been reported as excellent plasmonic catalysts among this class of structure and systems [19–21]. It successfully protects the Ag core, which has a respectable price, and has a large active interface between the semiconductor and noble metal. Wu et al. synthesized Ag-Cu_2O core-shell nanoparticles and discussed the mechanism of their enhanced photocatalytic activity [22]. However, the synthesized nanoparticles have the relatively large size (31–100 nm) and the stability of the catalyst has yet to be evaluated. Several reports have studied the stability of Cu_2O nanoparticles under ambient conditions or in water [23–25]. However, the stability of the Ag-Cu_2O core-shell nanoparticles under investigation.

Here in, we have prepared Ag-Cu_2O core-shell nanoparticles with bumpy structures using a very simple co-reduction method. The shell thickness was controlled to find optimum condition. The photocatalytic performance of the nanoparticles was evaluated using the methyl orange (MO) degradation method with changing shell thickness. The optical properties and the surface area of the nanoparticles played a key role in the photocatalytic performance. Furthermore, the stability of the nanoparticles after the photocatalytic reaction was investigated using a combined experimental and theoretical approach.

* Corresponding author.
E-mail address: hmlee@kaist.ac.kr (H.M. Lee).

http://dx.doi.org/10.1016/j.cattod.2017.08.016
Received 4 June 2017; Received in revised form 31 July 2017; Accepted 7 August 2017
Available online 09 August 2017
0920-5861/

2. Experimental methods

2.1. Materials and preparation of Ag-Cu_2O core-shell bumpy nanoparticles

Ag-Cu_2O core-shell bumpy nanoparticles were synthesized using the following facile, one-step co-reduction process. $AgNO_3$ (Sigma-Aldrich) was used as the silver precursor; copper acetylacetonate ($Cu(acac)_2$) ($Cu(C_5H_7O_2)_2$, Sigma-Aldrich) was used as the copper precursor; and oleylamine ($C_{18}H_{37}N$, Sigma-Aldrich) was used as the solvent, surfactant, and reducing agent. All chemicals were used as received without further purification. In the synthetic procedure, Ag-Cu_2O core-shell bumpy nanoparticles were synthesized with various Cu to Ag molar ratio (2:1, 4:1, and 8:1) using the co-reduction method. In this manner, $Cu(acac)_2$ (0.514 g, 1.028 g, and 1.542 g), $AgNO_3$ (0.16 g), and oleylamine (180 ml) were added to a 250-ml three-neck flask. The flask was heated to 230 °C and kept under high purity Ar gas with constant stirring for 3 h. The solution color changed from green to black when the co-reduction process was complete. The solution containing the synthesized nanoparticles was then cooled down to room temperature. The Ag-Cu_2O core-shell bumpy nanoparticles were obtained after centrifuging at 10000 rpm for 30 min and washed three times with hexane (C_6H_{14} < 96.0%, Junsei Chemical). Lastly, the powdered nanoparticles were obtained by drying under low vacuum at 40 °C for 24 h.

2.2. Characterization of the Ag-Cu_2O core-shell bumpy nanoparticles

The morphology and size distribution of the nanoparticles were investigated using transmission electron microscopy (TEM) (Tecnai G2 F30 S-Twin, FEI) at 300 kV. The core-shell bumpy structure was confirmed using high resolution transmission electron microscopy (HRTEM) and energy dispersive spectroscopy (EDS) (JEM-ARM200F, JEOL). The composition of the nanoparticles was also determined using EDS analysis. The crystalline structure was investigated using X-ray diffraction (XRD) (D/MAX-2500, RIGAKU) and the existence of the Cu_2O phase was verified using X-ray photoelectron spectroscopy (XPS) (K-alpha, Thermo VG Scientific). The optical properties of ethanol solutions containing the nanoparticles were investigated using a UV–vis spectrophotometer (Lambda 1050).

2.3. Measurement of photocatalytic activity

The photocatalytic activity was measured by the degradation of a methyl orange aqueous solution under the irradiation of visible-light at ambient condition. The commercial halogen lamp (500 W, Osram) was used as the visible-light source to induce the photocatalytic reaction. The distance between the solution and the light source was 20 cm. The temperature of the 500-ml beaker containing the MO solution was consistently maintained using a water chilling system. A total of 1.0 g powder of the synthesized Ag-Cu_2O core-shell bumpy nanoparticles as well as various Cu to Ag molar ratios were dispersed in 100 ml (10 mg/L methyl orange) aqueous solutions and were ultra-sonicated for 10 min. The solutions were stirred for 2 h in the dark to obtain the adsorption-desorption equilibrium. The solutions were then exposed to visible-light irradiation with constant stirring. At each time interval, 7 ml of the solution was collected using a syringe and centrifuged to remove the nanoparticles. The concentration of MO in the centrifuged solution was analyzed using a UV–vis spectrophotometer (Lambda 1050), and the characteristic absorption of MO at 464 nm was used to calculate its degradation rate. The degradation rate was calculated by $(C_0\text{-}C)/C_0$, where C is the adsorption of the MO solution at each time interval, and C_0 is the adsorption of initial MO immediately after the adsorption-desorption equilibrium.

2.4. Computational procedure

We performed GGA-level spin-polarized density functional theory (DFT) calculations with plane-wave based on a Vienna ab-initio simulation package (VASP) code [26]. The BEEF-vdw exchange correlation functional [27] was employed to describe interface phenomena and adhesion forces between metal (oxide) and metal oxide due to the consideration of Van der Waals interactions. Cut off energy was set to 500 eV, k-point sampling was chosen with gamma point, and convergence criteria for electronic structure and atomic geometry optimization were set to 10^{-5} eV and 0.05 eV/Å, respectively. We made 3 different slab systems Ag (111), Cu_2O (111), CuO (111) as a reference (Fig. S3). Each of systems are expanded to 4 × 4 supercell with 6 layers and bottom 4 layers are fixed in their bulk positions. All the slabs are centered between 10 Å vacuum layer. To describe the stability of copper oxide shell on the Ag core, we calculated adhesion force of CuO and Cu_2O layer when it forms interface with Ag or Cu_2O surfaces. Adhesion force is calculated by below equation.

$$E_{ad} = E_{total} - (E_{core} + E_{shell})$$

where E_{ad} is adhesion force, E_{total} is total energy after interface is formed, E_{core} is bare surface (or core of nanoparticle), and E_{shell} is target layer (or shell of nanoparticle) forms interface with E_{core}. Negative sign of adhesion force represents thermodynamically stable because total energy after interface formation is lower than bare surface.

3. Results and discussion

The Ag-Cu_2O core-shell nanoparticles with bumpy structures were synthesized using a very simple co-reduction method. According to our previous works, Cu^{2+} and Ag^{+} ions have vastly different reduction temperatures when using oleylamine as a reducing agent [28–30]. $Cu(acac)_2$ can be reduced over 180 °C, whereas $AgNO_3$ can be reduced at 80 °C. The considerable difference in the reducing temperatures allows for the synthesis of the Ag-Cu_2O nanoparticles with a core-shell structure using the proposed co-reduction method. While increasing the temperature to reach the desired reaction temperature, the Ag core is first reduced at a lower temperature and the Cu_2O shell is reduced at a higher temperature. These sequential reduction processes allow for the formation of the nanoparticles core-shell structure. We gradually increased the Cu to Ag molar ratio (2:1, 4:1, and 8:1) to control the shell thickness. Fig. 1 shows TEM images of the synthesized nanoparticles and their size distributions. The average size for the Ag nanoparticles was 11.0 nm ($\sigma \leq 12.6\%$). As the amount of Cu precursor increased, the average Ag-Cu_2O core-shell nanoparticle sizes were are 16.8 nm ($\sigma \leq 6.1\%$), 19.1 nm ($\sigma \leq 6.9\%$) and 22.0 nm ($\sigma \leq 7.9\%$) for the molar ratios (2:1, 4:1, and 8:1) respectively. The sizes of the nanoparticles are much smaller than those of previous reports [19,22,31]. The shell thickness was measured by subtracting the size of the Ag nanoparticles from the size of the Ag-Cu_2O core-shell bumpy nanoparticles. The measured shell thicknesses are 5.8 nm, 8.1 nm and 11.0 nm for each molar ratio. It can be shown that the shell thickness of the nanoparticles is successfully controlled by the facile co-reduction method with different Cu to Ag molar ratio. In this study, we designated the sample names as Ag-Cu_2O(2:1), Ag-Cu_2O(4:1) and Ag-Cu_2O(8:1). Additionally, the HRTEM images indicate that the Ag-Cu_2O core-shell nanoparticles have a multi-seeded structure for the Cu_2O shell, as shown in Fig. 2. It can be clearly seen that the shell thickness gradually grows as the molar ratio is increased. The core-shell structure could be checked from the lattice spacing measured in the HRTEM images. To confirm the core-shell structure of the nanoparticles more distinctly, the EDS line scanning and EDS elemental mapping were conducted. Fig. 3 shows the EDS analysis on Ag-Cu_2O(8:1) nanoparticles, presenting a clear core-shell structure.

Cu_2O has a +1 oxidation state and is a meta-stable state, spontaneously oxidizing to CuO or $Cu(OH)_2$. Therefore, we have attempted to confirm whether the synthesized nanoparticles consist of Cu_2O or other forms. The binding energy in XPS analysis is changed significantly according to the oxidation state of the species. In case of copper, the Cu^{+}

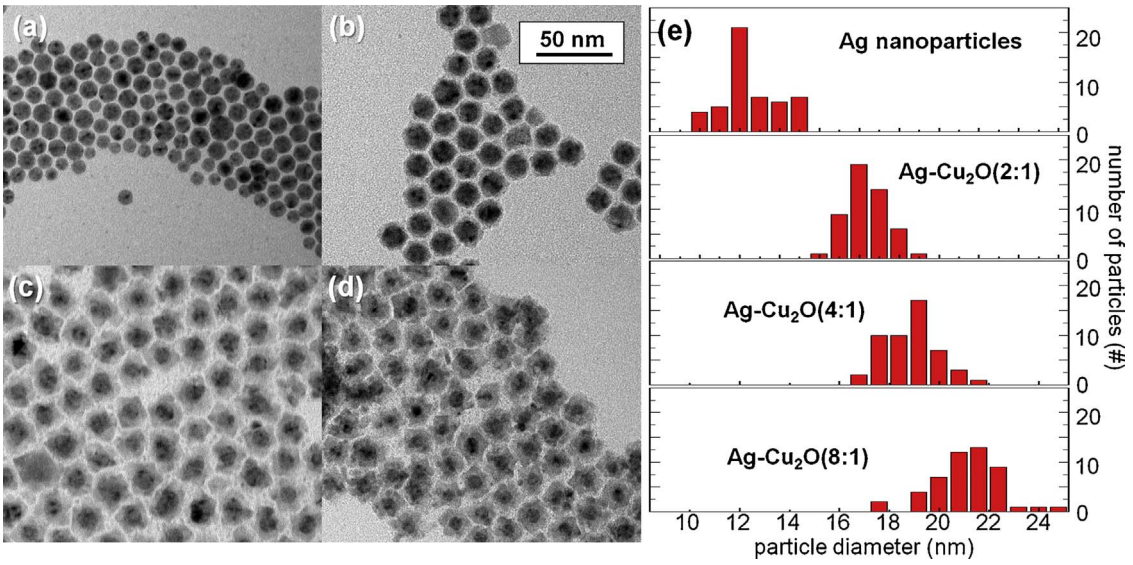

Fig. 1. TEM images of the synthesized nanoparticles (a) Ag, (b) Ag-Cu_2O(2:1), (c) Ag-Cu_2O(4:1), and (d) Ag-Cu_2O(8:1), and (e) their size distributions.

$2p_{3/2}$ peak position is approximately 932.2 eV. Cu^{2+} $2p_{3/2}$ for CuO, but has 933.6 eV that binds electrons stronger than the Cu^{+} phase [32]. Furthermore, the O1s peak position is approximately 531.0 eV [33]. O1s for Cu_2O and CuO are positioned at 530.2 eV and 529.5 eV, respectively [32]. Fig. 4 shows the curve-fitted XPS analysis of the Ag-Cu_2O(8:1) nanoparticles. The $Cu(OH)_2$ was not detected. The CuO phase was negligible, as shown in the Cu $2p_{3/2}$ and O 1s peaks. Additionally, the satellite peaks [34] for the Cu^{2+} oxidation state, generally appearing in higher binding energy compared to the $2p_{3/2}$ peak, are not detected. The quantitative compositions were calculated based on the area of peak deconvolution for Cu^{+}, Cu^{2+}, O in Cu_2O and O in CuO. The calculated compositions are Cu^{+}: Cu^{2+} = 95.3: 4.70 (at.%) and O in Cu_2O: O in CuO = 97.4: 2.59 (at.%). Additionally, we conducted XRD analysis on the Ag-Cu_2O core-shell bumpy nanoparticles to confirm the chemical state and crystalline structure. As expected, the peak intensities corresponding to Cu_2O were gradually increasing with increasing shell thickness. The relative peaks for Ag, on the other hand, were getting smaller. Other oxides or hydroxides of Cu were not

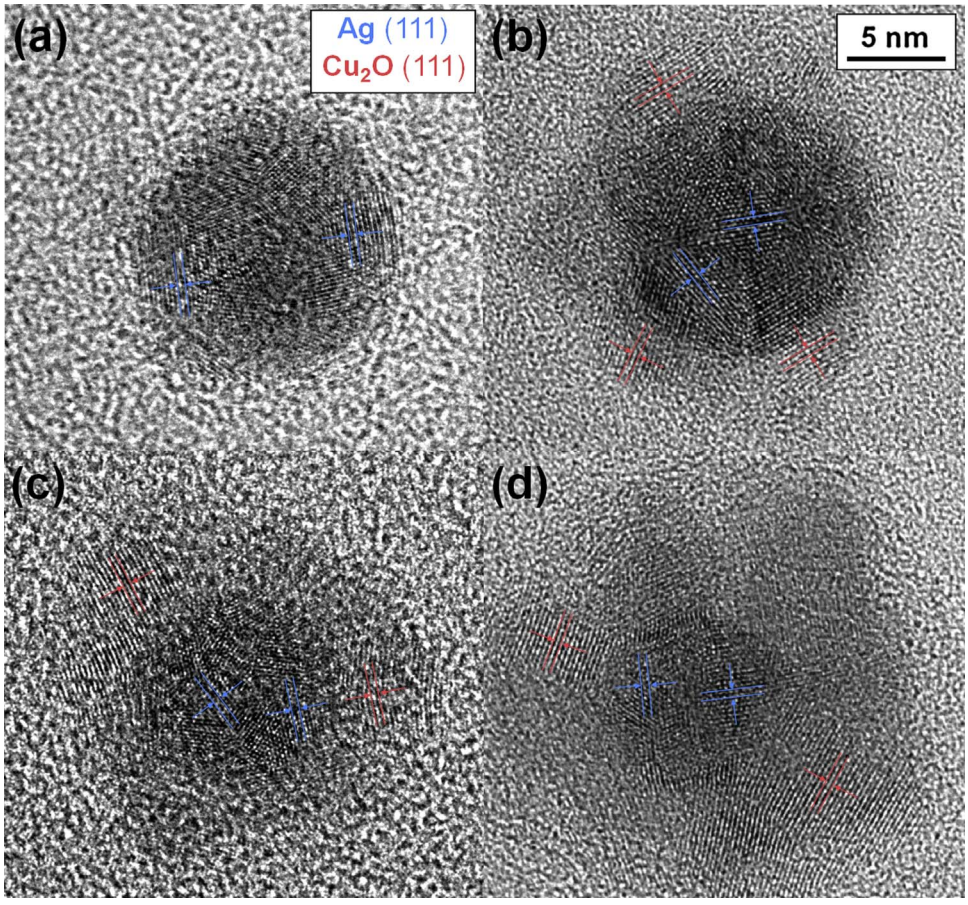

Fig. 2. HRTEM images of the synthesized nanoparticles: (a) Ag, (b) Ag-Cu_2O(2:1), (c) Ag-Cu_2O(4:1) and (d) Ag-Cu_2O(8:1).

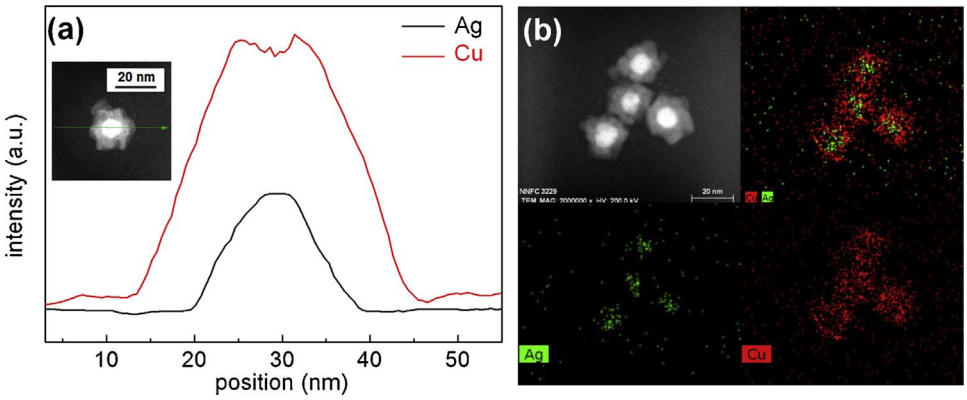

Fig. 3. (a) EDS line scanning of the Ag-Cu_2O(8:1) nanoparticles, (b) elemental mapping of the Ag-Cu_2O (8:1) nanoparticles.

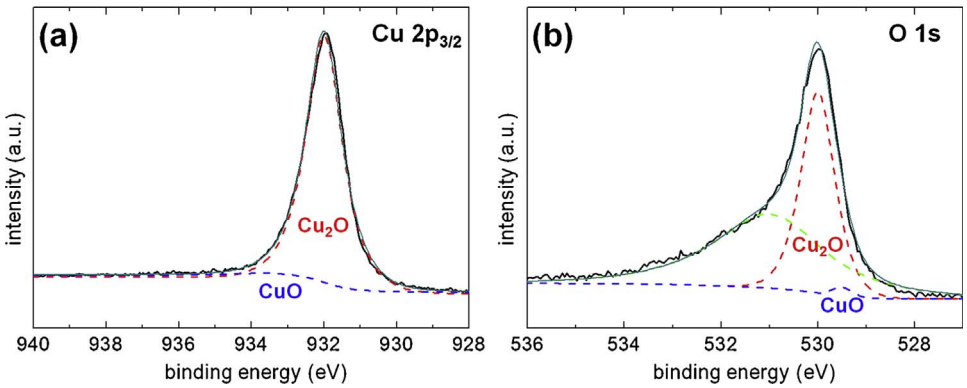

Fig. 4. (a) XPS Cu $2p_{3/2}$ spectrum and (b) XPS O 1s spectrum of the Ag-Cu_2O(8:1) nanoparticles.

detected. Actually, Cu^0 and Cu^{1+} states cannot be distinguished using only XPS analysis because Cu^0 and Cu^{1+} show almost the same binding energy. However, we were able to conclude that the nanoparticles consist of the Cu_2O and Ag phase because XRD data did not show any peak of the metallic Cu phase. From these two XPS and XRD analyses, it was confirmed that the Ag-Cu_2O core-shell bumpy nanoparticles consist of an almost pure Cu_2O phase at the shell and an Ag core.

The optical properties of the nanoparticles are some of the most important characteristics of the photocatalysts. Fig. 5(b) shows the UV–vis absorption spectroscopy of Ag, Cu_2O, Ag-Cu_2O(2:1), Ag-Cu_2O (4:1), and Ag-Cu_2O(8:1) nanoparticles. The red line indicates Cu_2O nanoparticles for comparison. The Cu_2O nanoparticles strongly absorb the light at a wavelength less than 450 nm. The absorption range for the Cu_2O nanoparticles is related to their bandgap (2.17 eV), as mentioned earlier. The Ag nanoparticles, represented by the black line, show strong absorption of light at approximately 480 nm. Although the SPR wavelength of the noble metals strongly depends on their shape, morphology and distribution [35], the absorption wavelength agrees well with several reports on Ag nanoparticles [36–39]. When the Cu_2O and Ag combined, all of the Ag-Cu_2O core-shell bumpy nanoparticles showed a much broader range of UV–vis absorption. The absorption of Ag-Cu_2O core-shell bumpy nanoparticles at the shorter wavelength gradually increased when shell thickness increased. It can be seen that the SPR wavelength for the Ag core is gradually red-shifted. According to several reports, the SPR wavelength can be red-shifted using dielectric materials around the noble metal nanoparticles [40,41]. Cu_2O is the dielectric material in this case. It can be expected that Ag-Cu_2O core-shell bumpy nanoparticles would have a better photocatalytic performance due to the broader absorption ranges.

The photocatalytic activities of the Cu_2O, Ag-Cu_2O(2:1), Ag-Cu_2O (4:1), and Ag-Cu_2O(8:1) nanoparticles were measured by the degradation of an MO aqueous solution under irradiation of light. At each interval (30 min), 7 ml of the solution was collected and centrifuged. The MO concentrations of the centrifuged solutions were measured using the characteristic absorption of MO. Fig. 6(a) shows the degradation rates of MO for each nanoparticle. The red line corresponds to the Cu_2O nanoparticles as a reference. The blue, green, and pink lines indicate the degradation rates of MO for Ag-Cu_2O(2:1), Ag-Cu_2O(4:1), and Ag-

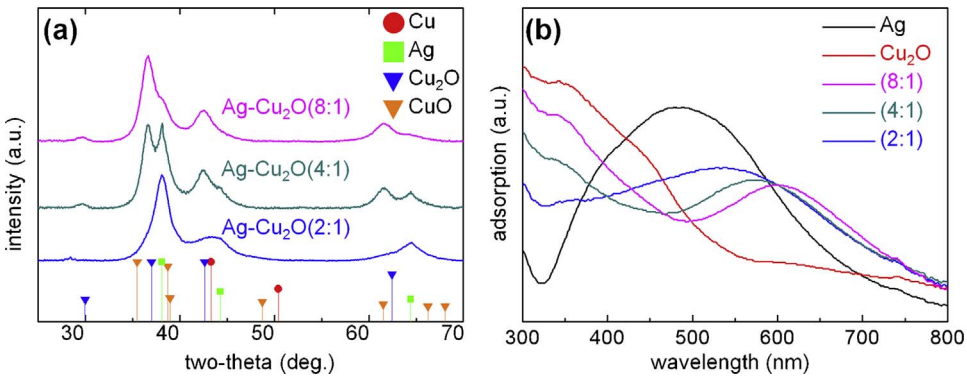

Fig. 5. (a) XRD analysis of the Ag-Cu_2O(2:1), Ag-Cu_2O(4:1), and Ag-Cu_2O(8:1) nanoparticles. (b) UV–vis absorption spectrum of the Ag, Cu_2O, Ag-Cu_2O(2:1), Ag-Cu_2O(4:1), and Ag-Cu_2O(8:1) nanoparticles.

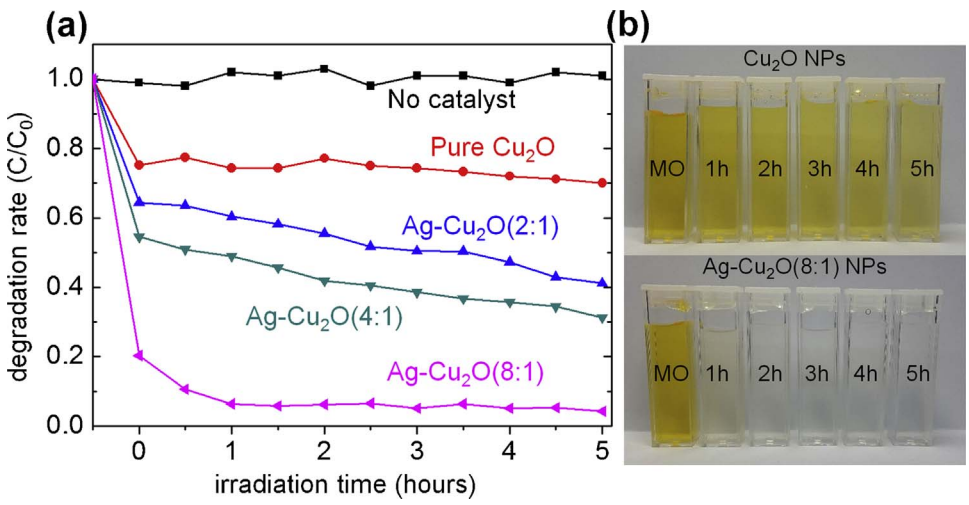

Fig. 6. (a) Degradation rate of MO via the photocatalysts: Cu_2O, Ag-Cu_2O(2:1), Ag-Cu_2O(4:1), and Ag-Cu_2O(8:1) nanoparticles. (b) Color changes of MO via the photocatalysts: pure Cu_2O and Ag-Cu_2O(8:1) nanoparticles.

Cu_2O (8:1) nanoparticles, respectively. It was evident that all of the core-shell nanoparticles had better photocatalytic activities compared to the reference. The activity trend is 'Cu_2O < Ag-Cu_2O (2:1) < Ag-Cu_2O (4:1) < Ag-Cu_2O (8:1)'. These enhanced properties could be explained by two factors: the SPR effect of Ag core and the high surface area of the unique bumpy structure.

The photoexcited energy can be transferred from noble metal to semiconductor with two mechanism: direct electron transfer (DET) [42–44] and plasmon-induced resonant energy transfer (PIRET) [45,46]. In the DET mechanism, the charge transfer can be from hot electrons generated by SPR in the noble metal, at which the hot electrons have at higher energy than the barrier between the semiconductor band edge and fermi level of the noble metal. Alternatively, the electric field generated by the dipole in the noble metal can induce a near-field electromagnetic interaction with the semiconductor in the PIRET mechanism, which allows for charge separation in the semiconductor. It is unclear which mechanism is dominant, however, Wu et al. have reported that both mechanisms can coexist in the case of Ag-Cu_2O core-shell nanoparticles [22].

It is necessary to investigate the surface area of the bumpy nanoparticles to elucidate the origin of enhanced photocatalytic activity. The Brunauer-Emmett-Teller (BET) surface area was measured for the nanoparticles, and the results are shown in Table S1. The surface area order is 'Ag-Cu_2O(2:1) < Cu_2O < Ag-Cu_2O(4:1) < Ag-Cu_2O(8:1)'. Owing to their smaller size, Cu_2O nanoparticles have slightly higher surface area than Ag-Cu_2O(2:1) nanoparticles. Other Ag-Cu_2O core-shell bumpy nanoparticles certainly have a much higher surface area compared to Cu_2O, although size increases. The high surface area of the Ag-Cu_2O nanoparticles can also be indirectly checked from the MO degradation rate shown in Fig. 6(a). Initial degradation rates at 0 h are related to the amount of MO adsorbed on the surface of the nanoparticles. The degradation rate at 0 h for Ag-Cu_2O(8:1) is the largest among all of the photocatalysts because it has the highest surface area.

The stability of the Cu_2O phase is as important as the photocatalytic activity because Cu_2O is in a meta-stable state. To investigate the shell thickness effect on the stability of the nanoparticles, their morphology and the oxidation state after the photocatalytic reaction were analyzed. Fig. 7(a) and (b) is TEM images for the Ag-Cu_2O(2:1) and Ag-Cu_2O(8:1) nanoparticles, respectively after the photocatalytic degradation of MO, showing very interesting results. The Cu_2O shells for Ag-Cu_2O(2:1) samples were detached from the Ag core shown in the arrows of Fig. 7(a). The detached Cu_2O nanoparticles and Ag core nanoparticles existed separately. As shown in Fig. 7(b), Ag-Cu_2O(8:1) nanoparticles maintain their original shape and morphology even after the reaction. The oxidation state of Ag-Cu_2O(2:1) and Ag-Cu_2O(8:1) nanoparticles after the reaction was also investigated, as shown in Fig. 7(c). The peak intensities (red arrow in Fig. 7(c)) of Cu^{2+} $2p_{3/2}$ and satellite peaks for Ag-Cu_2O(2:1), indicating the CuO (stable oxidation state), were largely increased compared to the intensities before the reaction in the Ag-Cu_2O(2:1) nanoparticles. Ag-Cu_2O(8:1) nanoparticles maintained their oxidation state as nearly the same before and after the reaction. Therefore, the Ag-Cu_2O(8:1) nanoparticles showed highest photocatalytic activity and stability simultaneously. The optimal thickness of Cu_2O in this research is 11.0 nm.

To elucidate this interesting shell thickness effects on the stability of Cu_2O, we conducted theoretical calculations using the Vienna ab-initio simulation package (VASP). We made simple model systems Ag-Cu_2O, Cu_2O-CuO, Ag-CuO (see Fig. 7(e)) to convince relation between stability and shell thickness of Cu_2O from the above experimental results. We attached Cu_2O and CuO single shell layer on the Ag core each to resemble change of Ag-Cu_2O(2:1) nanoparticle synthesized experimentally as reaction happens because oxidation states of thin Cu_2O shell is almost completely changed to that of CuO, and then CuO is detached from the Ag core. However, we attached CuO single shell layer on the Cu_2O core to design Ag-Cu_2O(8:1) because we assume that effect of Ag core be negligible when thickness of Cu_2O is enough. From these model systems, we calculated adhesion forces when interface is generated to figure out how the thickness of Cu_2O shell affects to the stability. Negative sign means stable and favorable to form the interface between two different systems. Interestingly, stable Cu_2O shell layer on the Ag (Ag-Cu_2O) is changed to drastically unfavorable after Cu_2O shell is transformed to CuO shell (Ag-CuO), and even in the geometrical figure of Ag-Cu_2O and Ag-CuO, we can find that well-ordered Cu_2O shell layer is totally collapsed after CuO shell is generated. Additionally, the weak adhesion force between Ag-CuO will cause detachment of CuO shell from the Ag core. In contrary to this, thick Cu_2O shell layer such as Ag-Cu_2O(8:1) can hold CuO shell layer although adhesion force is small, but still it has negative sign. We believe this adhesion force difference is due to the strain effect, thus we measured distance between two nearest metal atoms and compared distances between core and shell layer. We found there is strong relation between adhesion force and strain, and believe Cu_2O plays an important role as a buffer layer can hold both Ag and CuO layer which can increase the stability of nanoparticle. Although we discussed the thickness effect on the stability before and after the photocatalytic reaction using the experimental and theoretical methods, the long term stability is an issue to solve. It is not good because Cu_2O is in the meta-stable state as mentioned earlier. Doping or mixing may be the solution to enhance the long term stability. There is, however, still no reliable report about doping or mixing of Cu_2O except for a theoretical modeling on the mixed oxide phase of $(TiO_2)_x(CuO)_y$ [47].

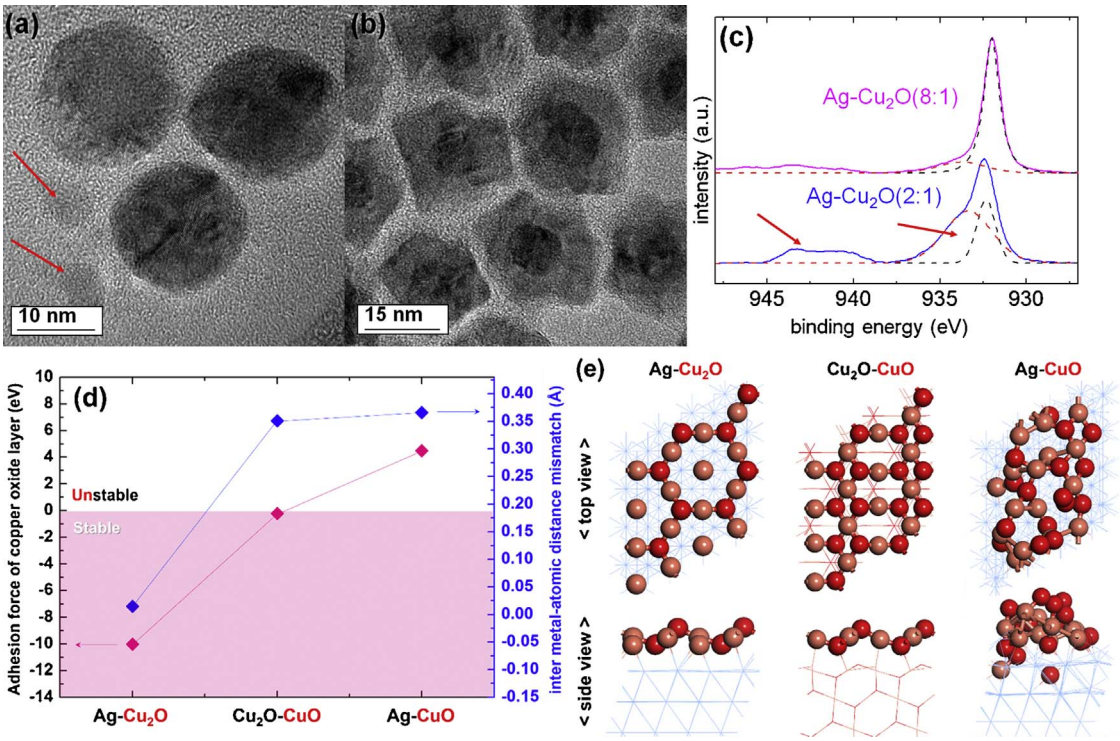

Fig. 7. TEM images of (a) Ag-Cu_2O(2:1) and (b) Ag-Cu_2O(8:1), and (c) XPS analysis of Cu $2p_{3/2}$ after photocatalytic reactions. (d) Adhesion forces of copper oxide layer on the different slab systems with magenta color and inter atomic distance mismatch between upper and lower layers with blue color, and (e) geometric structure of outmost layer on the different sublayers: Cu_2O layer on Ag surface (left), CuO layer on Cu2O surface (center), and CuO layer on Ag surface (right). (For interpretation of the references to colour in this figure legend, the reader is referred to the web version of this article.)

4. Conclusions

We have synthesized Ag-Cu_2O core-shell nanoparticles with bumpy structures using a very simple co-reduction method. The difference between the reducing temperatures of Cu_2O and Ag induced sequential reductions, leading to the core-shell structure. The synthesized nanoparticles showed a very pure Cu_2O phase of the shell, confirmed using XPS and XRD analyses. It was also evident that the nanoparticles show much broader absorption range of the UV–vis spectrum compared to that of pure Cu_2O. It was noted that the Ag-Cu_2O core-shell bumpy nanoparticles showed a red-shift of the SPR absorption with increasing shell thickness. This effect can be explained by the dielectric constant around the noble metal, in which the Cu_2O is the dielectric material in this case. Finally, we have tested the photocatalytic activity using the MO degradation and analyzed the stability after the photocatalytic reaction. As the shell thickness increased, the activity and stability are improved considerably. The enhanced activity originates from the high surface area of the bumpy structure and the plasmonic charge transfer from the Ag core. We have tried to explain the poor stability of Ag-Cu_2O (2:1) nanoparticles using DFT calculations. The theoretical study shows that the thin shell has a very large strain at the interface, leading to dewetting of the Cu_2O from the Ag core.

Acknowledgments

This research was supported by a National Research Foundation of Korea (NRF) grant funded by the Korean Government (MSIT) (No. NRF-2015R1A5A1037627).

Appendix A. Supplementary data

Supplementary data associated with this article can be found, in the online version, at http://dx.doi.org/10.1016/j.cattod.2017.08.016.

References

[1] M.R. Hoffmann, S.T. Martin, Chem. Rev. 95 (1995) 69–96.
[2] Q. Wang, T. Hisatomi, Q.X. Jia, H. Tokudome, M. Zhong, C.Z. Wang, Z.H. Pan, T. Takata, M. Nakabayashi, N. Shibata, Y.B. Li, I.D. Sharp, A. Kudo, T. Yamada, K. Domen, Nat. Mater. 15 (2016) 611–615.
[3] H. Takeda, K. Ohashi, A. Sekine, O. Ishitani, J. Am. Chem. Soc. 138 (2016) 4354–4357.
[4] J.M. Herrmann, Catal. Today 53 (1999) 115–129.
[5] P. Wang, B.B. Huang, Y. Dai, M.H. Whangbo, Phys. Chem. Chem. Phys. 14 (2012) 9813–9825.
[6] J. Pascual, J. Camassel, H. Mathieu, Phys. Rev. B 18 (1978) 5606–5614.
[7] H. Tang, H. Berger, P.E. Schmid, F. Levy, G. Burri, Solid State Commun. 87 (1993) 847–850.
[8] S.W. Cao, J.X. Low, J.G. Yu, M. Jaroniec, Adv. Mater. 27 (2015) 2150–2176.
[9] J.X. Low, J.G. Yu, W.K. Ho, J. Phys. Chem. Lett. 6 (2015) 4244–4251.
[10] R. Asahi, T. Morikawa, T. Ohwaki, K. Aoki, Y. Taga, Science 293 (2001) 269–271.
[11] F.X. Zhang, Y. Pi, J. Cui, Y.L. Yang, X. Zhang, N.J. Guan, J. Phys. Chem. C 111 (2007) 3756–3761.
[12] D. Chatterjee, Catal. Commun. 11 (2010) 336–339.
[13] G.K. Pradhan, S. Martha, K.M. Parida, ACS Appl. Mater. Interfaces 4 (2012) 707–713.
[14] M. Hara, T. Kondo, M. Komoda, S. Ikeda, K. Shinohara, A. Tanaka, J.N. Kondo, K. Domen, Chem. Commun. 3 (1998) 357–358.
[15] S.D. Sun, Nanoscale 7 (2015) 10850–10882.
[16] S. Kakuta, T. Abe, Electrochem. Solid-State Lett. 12 (2009) P1–P3.
[17] R. Sundararaman, P. Narang, A.S. Jermyn, W.A. Goddard, H.A. Atwater, Nat. Commun. 5 (2014) 5788.
[18] X.M. Zhang, Y.L. Chen, R.S. Liu, D.P. Tsai, Rep. Prog. Phys. 76 (2013) 046401.
[19] S.Q. Wei, J. Shi, H.J. Ren, J.Q. Li, Z.C. Shao, J. Mol. Catal. A Chem. 378 (2013) 109–114.
[20] H. Jing, N. Large, Q.F. Zhang, H. Wang, J. Phys. Chem. C 118 (2014) 19948–19963.
[21] J.Y. Xiong, Z. Li, J. Chen, S.Q. Zhang, L.Z. Wang, S.X. Dou, ACS Appl. Mater. Interfaces 6 (2014) 15716–15725.
[22] J.T. Li, S.K. Cushing, J. Bright, F.K. Meng, T.R. Senty, P. Zheng, A.D. Bristow, N.Q. Wu, ACS Catal. 3 (2013) 47–51.
[23] Y. Kwon, A. Soon, H. Han, H. Lee, J. Mater. Chem. A 3 (2015) 156–162.
[24] D. Dodoo-Arhin, M. Leoni, P. Scardi, E. Garnier, A. Mittiga, Mater. Chem. Phys. 122 (2010) 602–608.
[25] M.J. Siegfried, K.S. Choi, J. Am. Chem. Soc. 128 (2006) 10356–10357.
[26] G. Kresse, J. Furthmuller, Phys. Rev. B 54 (1996) 11169–11186.
[27] J. Wellendorff, K.T. Lundgaard, A. Mogelhoj, V. Petzold, D.D. Landis, J.K. Norskov, T. Bligaard, K.W. Jacobsen, Phys. Rev. B 85 (2012) 235149.
[28] C. Lee, N.R. Kim, J. Koo, Y.J. Lee, H.M. Lee, Nanotechnology 26 (2015) 455601.

[29] N.R. Kim, Y.J. Lee, C. Lee, J. Koo, H.M. Lee, Nanotechnology 27 (2016) 345706.
[30] N.R. Kim, K. Shin, I. Jung, M. Shim, H.M. Lee, J. Phys. Chem. C 118 (2014) 26324–26331.
[31] S. Tao, M. Yang, H.H. Chen, M.Y. Ren, G.W. Chen, J. Colloids Interfaces Sci. 486 (2017) 16–26.
[32] J. Ghijsen, L.H. Tjeng, J. Vanelp, H. Eskes, J. Westerink, G.A. Sawatzky, M.T. Czyzyk, Phys. Rev. B 38 (1988) 11322–11330.
[33] C.K. Wu, M. Yin, S. O'Brien, J.T. Koberstein, Chem. Mater. 18 (2006) 6054–6058.
[34] N.S. Mcintyre, M.G. Cook, Anal. Chem. 47 (1975) 2208–2213.
[35] N.E. Motl, A.F. Smith, C.J. DeSantis, S.E. Skrabalak, Chem. Soc. Rev. 43 (2014) 3823–3834.
[36] M. Chen, Y.G. Feng, X. Wang, T.C. Li, J.Y. Zhang, D.J. Qian, Langmuir 23 (2007) 5296–5304.
[37] M.S. Bootharaju, V.M. Burlakov, T.M.D. Besong, C.P. Joshi, L.G. AbdulHalim, D.M. Black, R.L. Whetten, A. Goriely, O.M. Bakr, Chem. Mater. 27 (2015) 4289–4297.
[38] N.G. Bastus, F. Merkoci, J. Piella, V. Puntes, Chem. Mater. 26 (2014) 2836–2846.
[39] Y. Lu, G.L. Liu, L.P. Lee, Nano Lett. 5 (2005) 5–9.
[40] L. Zhang, D.A. Blom, H. Wang, Chem. Mater. 23 (2011) 4587–4598.
[41] M.A. Mahmoud, M. Chamanzar, A. Adibi, M.A. El-Sayed, J. Am. Chem. Soc. 134 (2012) 6434–6442.
[42] Y. Tian, T. Tatsuma, J. Am. Chem. Soc. 127 (2005) 7632–7637.
[43] K. Wu, J. Chen, J.R. McBride, T. Lian, Science 349 (2015) 632–635.
[44] D.P. Wu, F.J. Wang, H.J. Wang, K. Cao, Z.Y. Gao, F. Xua, K. Jiang, Dalton Trans. 45 (2016) 16275–16282.
[45] S.K. Cushing, J.T. Li, F.K. Meng, T.R. Senty, S. Suri, M.J. Zhi, M. Li, A.D. Bristow, N.Q. Wu, J. Am. Chem. Soc. 134 (2012) 15033–15041.
[46] M. L-Viger, D. Brouard, D. Boudreau, J. Phys. Chem. C 115 (2011) 2974–2981.
[47] H.R. Liu, J.H. Yang, Y.Y. Zhang, S. Chen, A. Walsh, H. Xiang, X. Gong, S.H. Wei, Phys. Chem. Chem. Phys. 15 (2013) 1778–1781.